Biomaterials 35 (2014) 6164–6171

Contents lists available at ScienceDirect

Biomaterials

journal homepage: www.elsevier.com/locate/biomaterials

Ab initio molecular dynamics simulations of structural changes associated with the incorporation of fluorine in bioactive phosphate glasses

Jamieson K. Christie*, Richard I. Ainsworth, Nora H. de Leeuw

Department of Chemistry, University College London, 20 Gordon Street, London WC1H 0AJ, UK

ARTICLE INFO

Article history:
Received 25 February 2014
Accepted 10 April 2014
Available online 5 May 2014

Keywords:
Fluorine
Glass
Bioactive glass
Modelling
Bioactivity

ABSTRACT

Phosphate-based bioactive glasses containing fluoride ions offer the potential of a biomaterial which combines the bioactive properties of the phosphate glass and the protection from dental caries by fluoride. We conduct accurate first-principles molecular dynamics simulations of two compositions of fluorinated phosphate-based glass to assess its suitability as a biomaterial. There is a substantial amount of F–P bonding and as a result the glass network will be structurally homogeneous on medium-range length scales, without the inhomogeneities which reduce the bioactivity of other fluorinated bioactive glasses. We observe a decrease in the network connectivity with increasing F content, caused by the replacement of bridging oxygen atoms by non-bridging fluorine atoms, but this decrease is small and can be opposed by an increase in the phosphate content. We conclude that the structural changes caused by the incorporation of fluoride into phosphate-based glasses will not adversely affect their bioactivity, suggesting that fluorinated phosphate glasses offer a superior alternative to their silicate-based counterparts.

1. Introduction

Phosphate-based glasses [1] are increasingly used as biomaterials for implants in the body, owing to several valuable properties. Certain glass compositions are bioactive, that is, they react chemically when placed in a physiological environment. These glasses dissolve completely in aqueous environments, as found in the body, with a dissolution rate that varies over several orders of magnitude, dependent on composition [1,2]. Since these glasses can be synthesised using the ions normally found in the body, they have been employed in a wide range of biomedical applications [1,3], including fixation of bone fractures [4], tubular forms to aid neural repair [5] and the controlled release of antimicrobials [6] or drugs [7], among many others. Phosphate-based glasses are typically very soluble, and they also decompose to products which can be harmlessly eliminated by the body [1]. The addition of dopants and changes in composition allow for the possibility of tuning the dissolution rate to make the glass suited for a specific application. Although they have been less widely used clinically than other biomaterials [8], the increased solubility of phosphate-based glasses makes them eminently suitable for use as bioactive degradable materials, where the biomaterials or their dissolution products play an active role in tissue engineering.

Fluorine is used in dentistry where it has three beneficial effects: it enhances tooth enamel remineralisation, and inhibits demineralisation and the action of bacterial enzymes [9]. In particular, during enamel remineralisation in the presence of fluoride ions, the phosphate mineral fluorapatite is formed, which is much less susceptible to acid attack than hydroxyapatite, the primary constitutent of enamel. Fluoride-containing silicate-based bioactive glasses (BG) have been synthesised and are used in e.g. toothpaste for sufferers of dentine hypersensitivity. The structure and properties of fluorinated bioactive glasses (F-BG) have also been studied in experiment [10,11] and simulation [12–14]. The incorporation of fluorine into BG has deleterious effects on the bioactivity. During the formation of hydroxyapatite on F-free BG, a thick silica-rich gel layer is formed [15]. In vitro and in vivo studies show that this layer is less homogeneous on F-BG than on F-free BG [16], and under certain conditions is small or even absent [17,18]. The reason for this inhomogeneity has been identified as a structural one. Fluorinated silicate glasses show a very small amount of F–Si bonding [10,13] and hence a separation on medium-range length scales into

* Corresponding author.
E-mail address: jamieson.christie@ucl.ac.uk (J.K. Christie).

http://dx.doi.org/10.1016/j.biomaterials.2014.04.032

phosphosilicate-rich and Na/Ca/F-rich regions [12]. Ionic clustering is known to reduce bioactivity [19–21], and the surface reactivity of the glass will vary across the different regions, which is the likely cause of the disrupted formation of the silica gel layer.

Given this problem with fluorinated silicate BG, and the more controllable dissolution of phosphate-based bioactive glasses, it was logical to investigate fluorinated phosphate-based bioactive glasses (F-PBG) that would combine the beneficial effects of fluoride with superior bone bonding properties. Experimentally, it was found to be difficult to synthesise these glasses with consistent fluoride levels due to fluorine volatility [1], but the loss of fluoride could be controlled to a manageable level by minimising the use of P_2O_5.

In this work, we concentrate on the effects of incorporating fluorine on the structure, and hence the bioactivity, of phosphate-based glasses. Computer simulation is an ideal tool to investigate the structure and properties of glasses, as it allows us to understand material properties from the atomistic level, which is particularly useful for F-PBG due to the lack of experimental data. Simulation has been widely used to study the structures and properties of many different types of glasses [22–29], including those implanted into the body for biomedical reasons [19,20,30–32], as well as providing insight into the interactions of the glass with the physiological environment [33–35]. We use first-principles Born-Oppenheimer molecular dynamics (MD) simulations to create realistic, unbiased models of two phosphate glass compositions with different fluorine contents, where the interatomic forces are computed from a quantum-mechanical representation of the electronic structure. Although the high computational cost of this approach limits us to relatively small models, this disadvantage is offset by the high accuracy inherent in this parameter-free approach, which does not rely on the generation of an empirical force field. Models of diverse glass compositions prepared using first-principles MD have previously been used to complement experimental studies and provide vital information on the atomic structure and properties and their effect on the suitability of the different glasses for biomedical applications [13,36–38].

2. Materials and methods

Born-Oppenheimer molecular dynamics simulations were performed by the mixed plane-wave/Gaussian-basis-set CP2K code [39], using the generalised gradient approximation (GGA) to density-functional theory (DFT) with PBE exchange-correlation functionals [40]. All atomic species were represented using a double-zeta valence polarised (DZVP) basis set [41]. The plane-wave energy cutoff was 700 Ry, and the MD timestep was 1.0 fs. Periodic boundary conditions were used throughout.

Two compositions were modelled, based on the metaphosphate glass composition, one with 2 mol % CaF_2 (hereafter called F2) and one with 6 mol % CaF_2 (F6). The glass compositions were also chosen to have the same ratio of numbers of P atoms to O atoms as each other and as the reference metaphosphate composition. The precise compositions are given in Table 1. The densities of the fluorinated compositions were not obtainable experimentally, nor available via glass property modelling databases, and we have therefore estimated the effect on the density of incorporating fluorine to the metaphosphate composition, based on the fractional increase of density observed when fluorine was added to ternary silicate-based glasses by Brauer et al. [42] For the starting configurations, atoms were placed randomly and independently in a cubic periodic box subject only to the constraint that no two atoms were closer than about 80–90% of their expected interatomic separation. The size of the box was chosen to give the appropriate density (Table 1) and kept constant throughout the simulation. To ensure that there were sufficient fluorine atoms in each model to obtain reliable statistics of their structures, the F6 model contains 197 atoms, of which six are fluorine, but due to its lower F content, the F2 model contains 363 atoms, of which four are fluorine.

For each composition, an MD run was started from the initial quasi-random configuration in the NVT ensemble at 2500 K until the model was well equilibrated, which was confirmed by computing the actual and mean-square atomic displacements. This typically took 20 ps of MD simulation time. Then, each model was run for 10 ps in NVT ensembles at each of the following temperatures: 2200 K, 1900 K, 1600 K, 1300 K, 1000 K, 750 K and 500 K, before being run for 20–25 ps in the NVT ensemble at 300 K. The production run, overwhich all data given in this paper are averaged, constitutes the last two-thirds of this room-temperature run. This protocol corresponds to a total simulation time of 110 ps, and an effective cooling rate of just over 30 K ps^{-1}. Although this cooling rate is substantially faster than that used to prepare glasses experimentally, simulated cooling rates of this order of magnitude have been used to prepare accurate structural models of glasses in agreement with experimental results using first-principles [13,37,38] molecular dynamics, whereas even the cooling rates achieved in classical molecular dynamics simulations [22,29] are less than an order of magnitude slower.

Table 1
The simulated compositions (in CaF_2 mol %) and their densities and sizes. The fluoride-free F0 composition is included for reference.

Composition	P_2O_5	Na_2O	CaO	CaF_2	Density (g cm^{-3})	Number of atoms	Cell size (Å)
F0	50.0	20.0	30.0	0.0	2.585 [43]	Not simulated	
F2	49.0	19.6	29.4	2.0	2.593	363	17.0718
F6	47.0	18.8	28.2	6.0	2.610	197	13.9227

3. Results

The aim of this work is to characterise the atomic structure of fluorinated phosphate-based glasses, and the likely effect of the inclusion of fluorine on their bioactivity. The structures of various fluorine-free phosphate-based glasses with related compositions have already been characterised through simulation [29] and experiment [6,44–49], and in this section we will therefore concentrate on the structure around the fluoride ions.

Fig. 1 shows views of the simulated F2 and F6 compositions. The basic building block of the (F-free) phosphate glass network is the PO_4 tetrahedron. In a fully connected phosphate glass, three of the oxygen of each PO_4 group are bridging oxygen (BO) atoms which are also bonded to another PO_4 tetrahedron, whilst the fourth is a terminal oxygen (TO) atom, double-bonded to the phosphorus atom. The presence of modifier atoms like sodium and calcium causes P–O–P bonds to break, thereby forming non-bridging oxygen (NBO) atoms and fragmenting the network which increases the solubility.

3.1. Local environments of phosphorus

For both compositions, the first peak in the phosphorus–oxygen partial pair-correlation function, $g_{PO}(r)$ (Fig. 2(a)), occurs at similar distances and resolves the two types of P–O bonding: the shorter distance (bond length 1.50 Å) is the P-TO peak, and the larger (1.63 Å) is the P-BO peak, in agreement with previous simulations of F-free phosphate glasses [29]. Hoppe et al. [49] showed the experimental P–O bond lengths to be sensitive to the molar ratio $y = n(M_{2/\nu}O)/n(P_2O_5)$, where $n(x)$ is the molar content of moiety x, and ν is the charge of the modifier M. According to this observation [49], compositions with $y = 1.0$, like ours, have P-TO distances of 1.51 Å and P-BO distances of 1.62 Å, very close to those found in these simulations. In $g_{PF}(r)$ (Fig. 2(b)), only one peak at 1.58 Å is seen for both compositions, at distances intermediate to the two P–O bond lengths. In an F-free glass, the P–O coordination number would be exactly four, reflecting the tetrahedral structure around the P; however, in these glasses, we find a P–O coordination number slightly below four: 3.96 for F2 and 3.93 for F6. On examining $g_{PF}(r)$ and the P–F coordination numbers, which are 0.04 for F2 and 0.07 for F6, we see that a small amount of the oxygen atoms in the PO_4 tetrahedron have been replaced by fluorine atoms. The phosphorus atoms are essentially always (99.8% for F2, 100.0% for F6) four-coordinated when both oxygen and fluorine are taken into account. When P–F bonding occurs, one of the fluorine atoms takes the place of one of the oxygen atoms in a PO_4 unit,

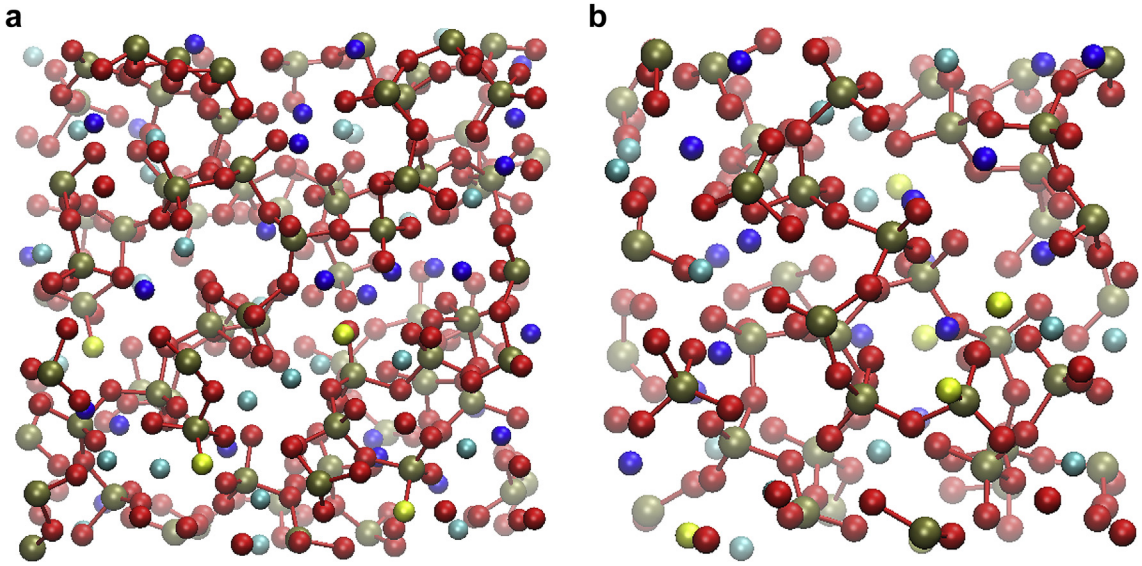

Fig. 1. Views of the (a) F2 and (b) F6 compositions. The colours are: phosphorus (brown), oxygen (red), sodium (dark blue), calcium (light blue), fluorine (yellow). (For interpretation of the references to colour in this figure legend, the reader is referred to the web version of this article.)

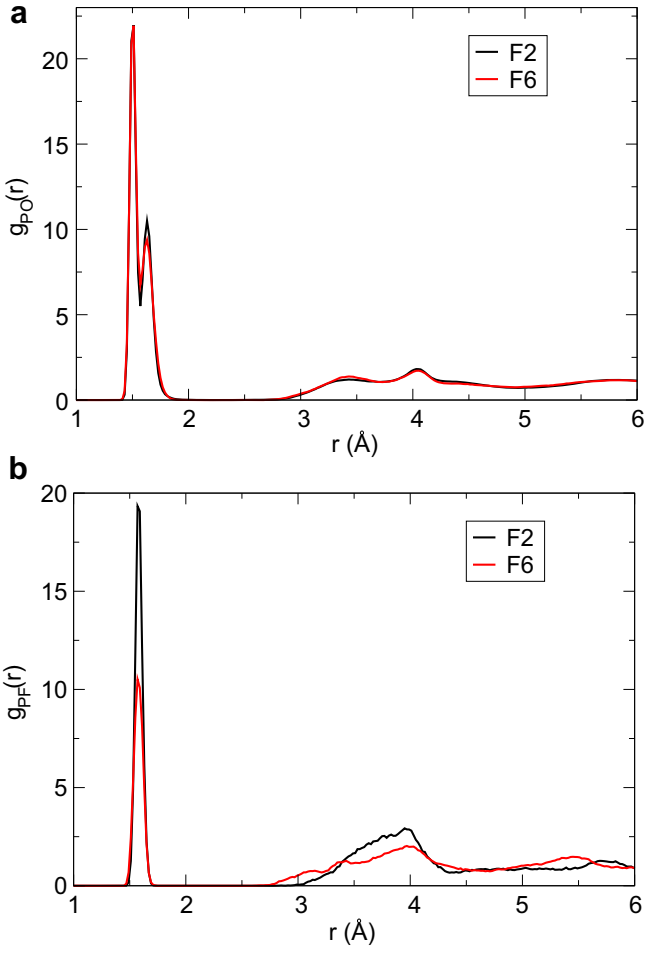

Fig. 2. Partial pair-correlation functions (a) $g_{PO}(r)$ and (b) $g_{PF}(r)$ for the F2 (black) and F6 (red) compositions. (For interpretation of the references to colour in this figure legend, the reader is referred to the web version of this article.)

creating a PO_3F tetrahedron instead. Fig. 3 shows representative examples of these structural units. No bridging F atoms were observed, that is, atoms in a P–F–P bridge; these are extremely unlikely to occur due to the F ion's single negative charge which would be unable to charge-balance two phosphorus atoms, unlike an oxygen atom with its double negative charge.

To underline the tetrahedral nature of the phosphate units, the O–P–O bond-angle distributions were computed (Fig. 4(a)), showing a distribution peak close to the ideal tetrahedral angle (109.5°) for both compositions. The O–P–F bond-angle distributions (Fig. 4(b)) peak at similar angles, but show a slight difference between the two compositions. The distribution for the F2 composition has a shoulder at angles of about 95°, which may be due to poor statistics, while that for the F6 composition is a single smooth peak as for the O–P–O distribution. The F2 composition typically has only nine O–P–F bond angles in the model, and even small fluctuations suffice to move the distribution away from a smooth monomodal peak. The tetrahedral environment of the phosphorus atoms is maintained.

3.2. Fluorine bonding and coordination numbers

In the F2 composition, three of the four fluorine atoms are bonded to a phosphorus atom, i.e. an F–P coordination number of 0.75, and in the F6 composition, three of the six fluorine atoms are so bonded, with an F–P coordination number of 0.5. Whilst we cannot define a reliable generic F–P coordination number due to the small number of fluorine atoms in each of our models, it is clear that the amount of F–P bonding is substantially larger than the amount of F–Si bonding in silicate-based bioactive glasses, which had a simulated F–Si coordination number of only 0.17 [13], whereas F–Si was not observed (i.e. coordination number of 0.0) in NMR spectra [10]. Based on our much larger calculated F–P coordination number, we predict that F–P bonding would be observed in NMR.

The fluorine-modifier bonding has a different character. For both compositions, the F–Na bond length is about 2.3 Å, and the F–Ca bond length is slightly shorter at about 2.2 Å for F2 and 2.25 Å for F6. The peaks in the corresponding partial pair-correlation functions, $g_{FNa}(r)$ and $g_{FCa}(r)$ (Fig. 5), are all broader than the typical F–P

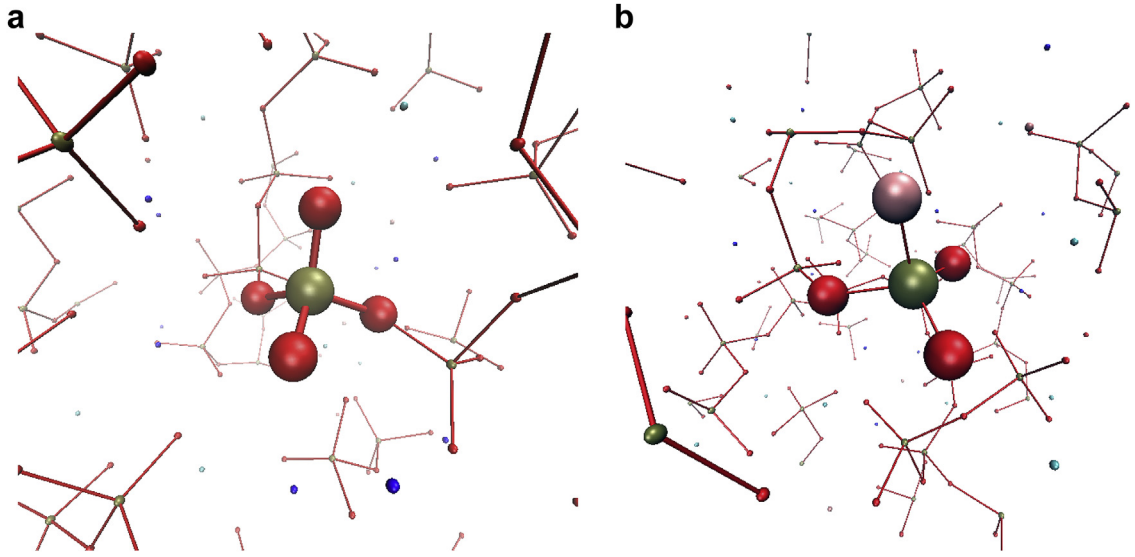

Fig. 3. Examples of (a) PO_4 and (b) PO_3F tetrahedra; surrounding atoms have been shrunk for clarity. (P atoms are gold, O red, F pink.) (For interpretation of the references to colour in this figure legend, the reader is referred to the web version of this article.)

peak, implying a wide range of coordination numbers and substantial disorder in the local environments. However, the small number of fluorine atoms and F–Na and F–Ca bonds again lead to substantial noise in the data.

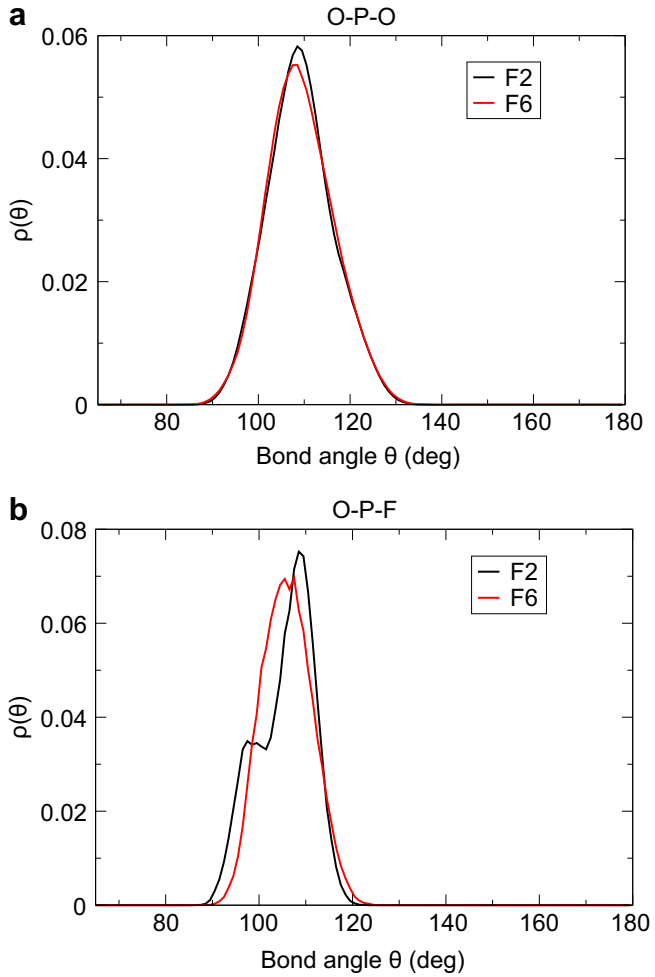

Fig. 4. The (a) O–P–O and (b) O–P–F bond-angle distributions.

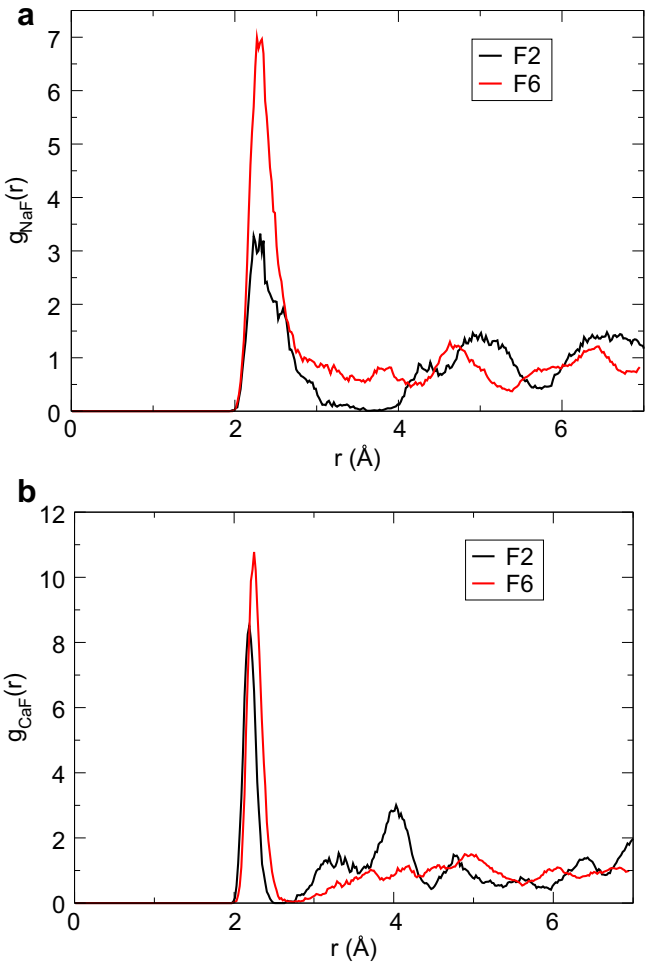

Fig. 5. Partial pair-correlation functions (a) $g_{NaF}(r)$ and (b) $g_{CaF}(r)$ for the F2 (black) and F6 (red) compositions. (For interpretation of the references to colour in this figure legend, the reader is referred to the web version of this article.)

Significant differences are observed between the F–Na and F–Ca bonding. The first peak in the partial pair-correlation function $g_{FCa}(r)$ is sharper than the equivalent peak in $g_{FNa}(r)$, implying that there is less variation in the F–Ca bond length than in the F–Na one (Fig. 5). The F–Ca peak also falls quickly to near zero, giving a good separation between the first and subsequent coordination shells. Using the first minimum in the partial pair-correlation functions as nearest-neighbour cutoffs (2.55 Å for F2 and 2.72 Å for F6), the F–Ca coordination number is 0.50 for F2 and 0.83 for F6. The F–Na peaks do not approach zero so closely, blurring the distinction between the first and subsequent neighbour shells, which in any case occurs at larger distances, namely 3.65 Å for F2, and 3.6 Å for F6. The F–Na coordination number is then 0.75 for F2, and 1.54 for F6.

The differences are largely attributable to the small number of F atoms in the models, and the large changes in the statistics that slightly different bonding environments produce. The fluorine bonding environments are given in Table 2. We see that fluorine atoms which are bonded to one phosphorus atom bind to modifiers in a substantially different manner compared to fluorine atoms that are not bonded to phosphorus. Fluorine atoms bonded to a phosphorus atom are also bonded to 0.67 (F2) and 0.88 (F6) sodium atoms but not to calcium atoms. The difference in P–F bonding between the models is enough to change the P-modifier coordination numbers substantially.

To underline this result, Mulliken charge analysis was performed on the fluorine atoms, and a substantial difference was found between fluorine atoms bonded to phosphorus and those not bonded to phosphorus. For both compositions, fluorine atoms bonded to phosphorus had Mulliken charges between −0.15 and −0.23, indicating substantial covalency in the F–P bond. Those fluorine atoms not bonded to phosphorus, i.e. only to modifiers, are much more ionic in character, with Mulliken charges between −0.63 and −0.73. Fig. 6 shows an isosurface of the electrostatic potential around anions in a PO_3F tetrahedron. Very little difference is seen between the potential around the oxygen atom or the fluorine atom, implying that the covalent character of the P–O and P–F bonds is similar.

3.3. Modifier atoms bonding

Table 3 shows the Na and Ca coordination numbers taking account of both oxygen and fluorine in the first coordination shell. The coordination numbers are between 6.1 and 7.2, taking into account coordination to both oxygen and fluorine, with six and seven as the most common coordination numbers for both sodium and calcium. Fig. 7 shows the O–M–O, O–M–F and F–M–F bond-angle distributions, where M is either of the modifiers Na or Ca. The O–M–O and O–M–F distributions follow the same broad shape with a main peak at 80° and a secondary peak at 140°. The F–M–F distributions correspond to a very small number of instances, and are included here for completeness. These distributions imply that the structure of the first coordination shell around the modifier

Table 2
The local fluorine environments, and their abundances, in the models studied.

Environment	F2	F6
FPNa	50%	44%
FP	25%	3%
$FNaCa_2$	25%	12%
FNa_2Ca_2	0	21%
FNa_3Ca	0	17%
$FPNa_2$	0	3%
other	0	0.5%

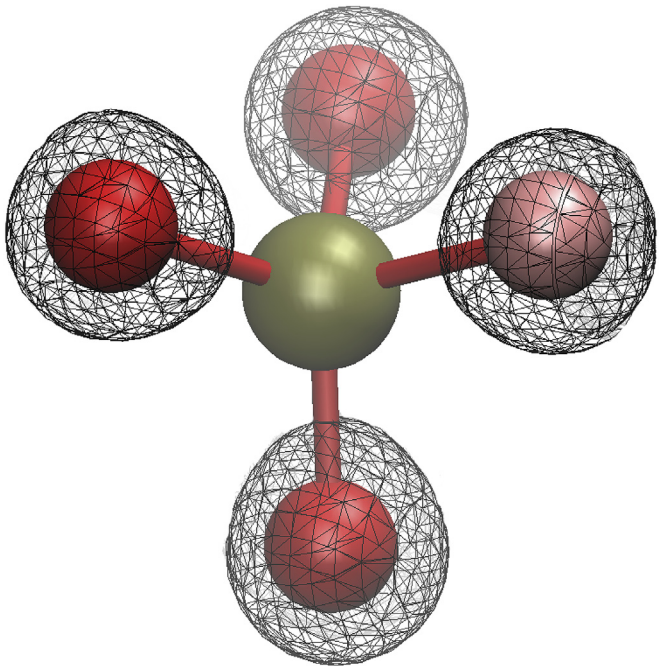

Fig. 6. The $q = 0.3e$ isosurface of the electrostatic potential around oxygen (red) and fluorine (pink) atoms bonded to a central phosphorus atom. Other atoms and electrostatic information around them have been removed for clarity. (For interpretation of the references to colour in this figure legend, the reader is referred to the web version of this article.)

atoms is a distorted octahedron. A perfect octahedron would show bond angles at 90 and 180°; since the average coordination number of the modifier atoms is slightly larger than six, geometric constraints mean that these bond angles would shrink slightly. Sodium, with its lower field strength than calcium, has a peak in its O–Na–O bond-angle distribution at about 60°, corresponding to two oxygen atoms bonded to the same phosphorus atom, or so-called “intra-tetrahedral” bonding [32,50].

3.4. Network connectivity and the Q^n distribution

One of the main atomistic properties which affects the bioactivity of a glass is the network connectivity (NC) and the associated Q^n distribution [19]. A network-forming cation, phosphorus in these glasses, is Q^n if it has n bridging oxygen atoms which connect one PO_4 tetrahedron to another. NC is obviously a sensitive function of composition, and the presence of modifier cations will alter the Q^n distribution considerably, typically pushing the distribution to lower values, and so reducing the network connectivity, which is the mean value of n [19]. Although the small size of these models

Table 3
The Na-T and Ca-T coordination numbers, where T = O or F.

	Na		Ca	
CN	F2	F6	F2	F6
4	4%	2%	–	–
5	22%	13%	1%	7%
6	40%	30%	16%	37%
7	27%	39%	48%	41%
8	6%	12%	32%	15%
9	1%	4%	2%	1%
M-O	6.02	6.01	7.12	6.32
M-F	0.10	0.58	0.08	0.33

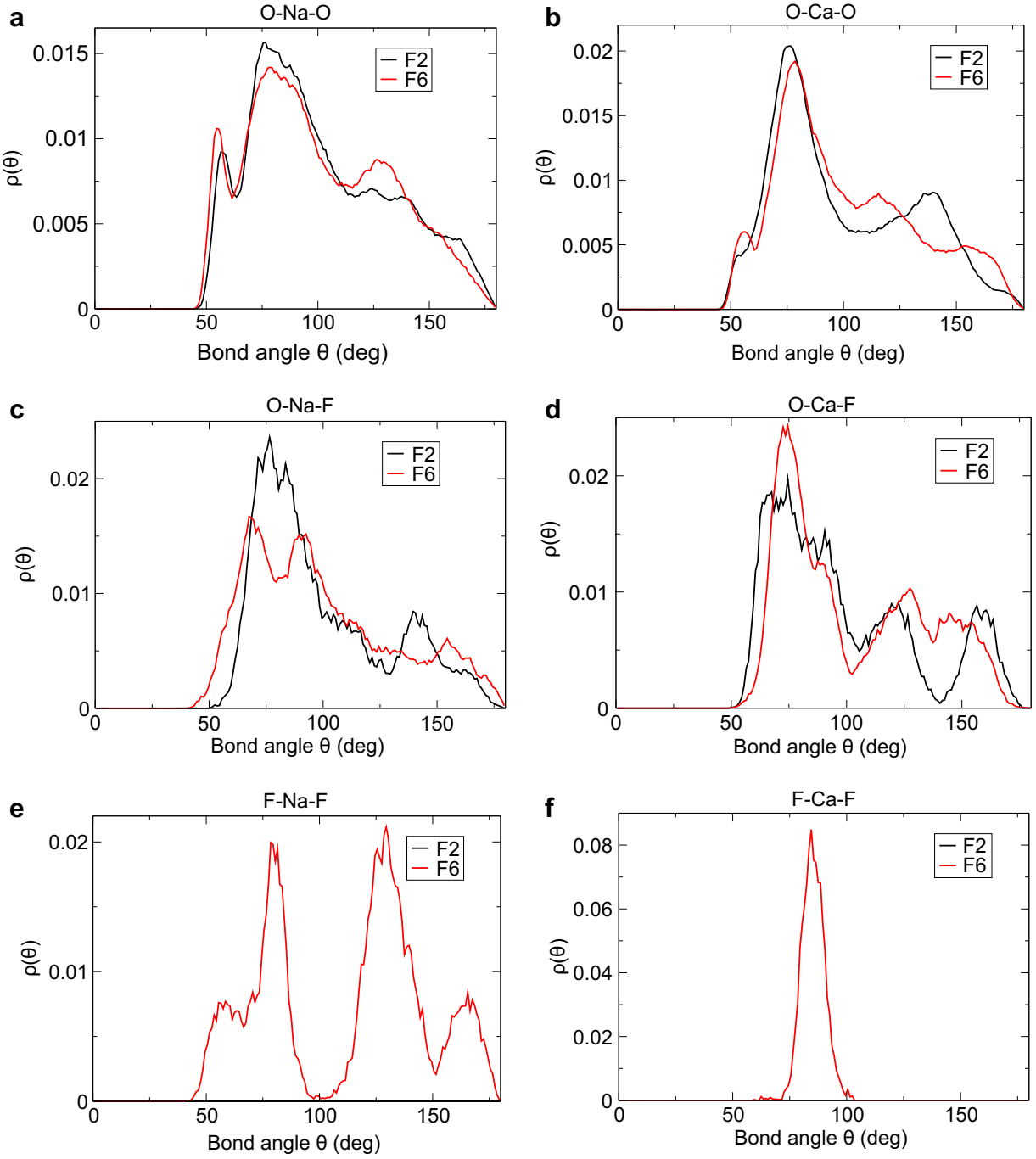

Fig. 7. The (a) O–Na–O, (b) O–Ca–O, (c) O–Na–F, (d) O–Ca–F, (e) F–Na–F and (f) F–Ca–F bond-angle distributions for the F2 (black) and F6 (red) compositions. (For interpretation of the references to colour in this figure legend, the reader is referred to the web version of this article.)

and the concomitant small number of fluorine atoms affect any quantitative predictions, it is still important to discuss the connectivity of the networks in the models, particularly bearing in mind that the compositions were constructed to have the same ratio of numbers of O atoms to P atoms. The Q^n distributions and network connectivities are given in Table 4. We see that, for both compositions, the majority of phosphorus atoms are Q^2 with small proportions of Q^1 and to a lesser extent Q^3, implying a structure made up mostly of phosphate chains with few branches, while there is a slight decrease in the network connectivity with increasing F content (the F-free F0 metaphosphate composition has a network connectivity of 2.0).

4. Discussion

We have computed the changes in the structure of phosphate-based glasses brought about by the inclusion of fluorine, to establish how this doping affects the suitability of these glasses for biomedical implantation. We have shown that there is a significant amount of P–F bonding, and that where this occurs the fluorine atom replaces one of the oxygen atoms in a P–O bond, preserving the tetrahedral structure around the phosphorus atoms. We have also observed a decrease in the network connectivity with increasing fluorine content, which we suggest, is due to the lack of bridging fluorine atoms, because of the fluorine's single negative

Table 4
The Q^n distributions, and the network connectivities (NC), in the models studied.

n	F2	F6
0	0.2%	–
1	17%	23%
2	74%	70%
3	9%	8%
NC	1.92	1.85

charge. Increasing the fluorine content increases the P–F coordination number (and decreases the P–O coordination number) and hence decreases the network connectivity.

A decrease in network connectivity will typically increase the bioactivity of a glass by making the network more fragmented and more soluble. We have seen in other glasses [32,50] that a decrease in network connectivity caused by the increase in some active modifying component can be compensated by increasing the content of the network former, phosphate in this case. Since the decrease in network connectivity is rather small (2.0–1.84) even with moderate (6 mol %) amounts of CaF_2, it seems likely that any undesirable increase in solubility for a given application could be countered by an increase in the phosphate content, enabling the network connectivity to be tuned to that required for the specific application.

The network connectivity is not the only structural parameter which affects the bioactivity. In the case of fluorinated silicate bioglasses, it is clear from experiment [10], classical [12] and first-principles [13] simulations that fluorine overwhelmingly prefers to bond to the modifier atoms, sodium and calcium, leading to segregation of the glass into modifier-rich and phosphosilicate-rich regions on length scales of several nearest neighbours. Clustering of modifier atoms is associated with more durable, less bioactive glass networks [20,21], and experimentally the formation of the silica gel layer during reaction of these glasses with the physiological surroundings was disrupted, reduced or missing [16,18], with associated changes in the surface reactivity compared to the F-free glass [12,17].

In contrast, in the case of the fluorinated phosphate glasses studied here, the order of magnitude of the F–P coordination numbers is much the same as for the F–Na and F–Ca coordination numbers. This implies that any such mesoscale segregation will be much smaller and less important and that the observed reduction in bioactivity in fluorinated silicate-based bioglass will not occur in the fluorinated phosphate-based glass.

5. Conclusion

We conclude, therefore, that there are likely to be two effects on the bioactivity of phosphate glasses caused by the incorporation of fluorine. The first, where the replacement of an oxygen atom in a PO_4 tetrahedron by a non-bridging fluorine atom causes a slight reduction in the glass network connectivity, is likely to increase the bioactivity, but only to such an extent that it can be corrected for any reasonable amount of fluorine content. The second effect, namely the segregation of the glass network into modifier-rich and network-rich regions with an attendant decrease in bioactivity, is likely to be insignificant due to the sizable amount of P–F bonding observed. We propose, therefore, that fluorinated phosphate-based glasses will not suffer the same decrease in bioactivity as fluorinated silicate-based glasses, and that fluorinated phosphate-based glasses are strong candidates for biomaterials with a dissolution rate tunable to specific biomedical applications, and with the added benefits that fluorine incorporation brings.

Acknowledgements

We acknowledge the EPSRC (grant no. EP/J008095/1) for funding. Via our membership of the UK's HPC Materials Chemistry Consortium, which is funded by EPSRC (grant nos. EP/F067496 and EP/L000202), this work made use of the facilities of HECToR, the UK's national high-performance computing service.

References

[1] Knowles JC. Phosphate based glasses for biomedical applications. J Mater Chem 2003;13:2395–401.
[2] Ahmed I, Lewis M, Olsen I, Knowles JC. Phosphate glasses for tissue engineering: part 1. Processing and characterisation of a ternary-based P_2O_5-CaO-Na_2O glass system. Biomaterials 2004;25:491–9.
[3] Lakhkar NJ, Lee I-H, Kim H-W, Salih V, Wall IB, Knowles JC. Bone formation controlled by biologically relevant inorganic ions: role and controlled delivery from phosphate-based glasses. Adv Drug Deliv Rev 2013;65:405–20.
[4] Uo M, Mizuno M, Kuboki Y, Makishima A, Watari F. Properties and cytotoxicity of water soluble Na_2O-CaO-P_2O_5 glasses. Biomaterials 1998;19:2277–84.
[5] Gilchrist T, Glasby MA, Healy DM, Kelly G, Lenihan DV, McDowall KL, et al. In vitro nerve repair – in vivo. The reconstruction of peripheral nerves by entubulation with biodegradeable glass tubes – a preliminary report. Br J Plast Surg 1998;51:231–7.
[6] Valappil SP, Pickup DM, Carroll DL, Hope CK, Pratten J, Newport RJ, et al. Effect of silver content on the structure and antibacterial activity of silver-doped phosphate-based glasses. Antimicrob Agents Chemother 2007;51:4453–61.
[7] Pickup DM, Newport RJ, Knowles JC. Sol-gel phosphate-based glass for drug delivery applications. J Biomater Appl 2012;26:613–22.
[8] Sculean A, Barbe G, Chiantella GC, Anweiler NB, Berakdar M, Brecx M. Clinical evaluation of an enamel matrix protein derivative combined with a bioactive glass for the treatment of intrabony periodontal defects in humans. J Periodontol 2002;73:401–8.
[9] Featherstone JDB. The science and practice of caries prevention. J Am Dent Assoc 2000;131:887–99.
[10] Brauer DS, Karpukhina N, Law RV, Hill RG. Structure of fluoride-containing bioactive glasses. J Mater Chem 2009;19:5629–36.
[11] Brauer DS, Karpukhina N, O'Donnell MD, Law RV, Hill RG. Flouride-containing bioactive glasses: effect of glass design and structure on degradation, pH and apatite formation in simulated body fluid. Acta Biomater 2010;6:3275–82.
[12] Lusvardi G, Malavasi G, Tarsitano F, Menabue L, Menziani Mc, Pedone A. Quantitative structure-property relationships of potentially bioactive fluoro phospho-silicate glasses. J Phys Chem B 2009;113:10331–8.
[13] Christie JK, Pedone A, Menziani MC, Tilocca A. Fluorine environment in bioactive glasses: *ab initio* molecular dynamics simulations. J Phys Chem B 2011;115:2038–45.
[14] Pedone A, Charpentier T, Menziani MC. The structure of fluoride-containing bioactive glasses: new insights from first-principles calculations and solid state NMR spectroscopy. J Mater Chem 2012;22:12599–608.
[15] Hench LL. Bioactive materials: the potential for tissue regeneration. J Biomed Mater Res 1998;41:511–8.
[16] Zaffe D, Krajewski A, Ravaglioli A, Contoli S. Study on short-term implants of a fluorinated glass in bone. J Mater Sci Mater Med 1993;4:169–74.
[17] Lusvardi G, Malavasi G, Menabue L, Aina V, Morterra C. Fluoride-containing bioactive glasses: surface reactivity in simulated body fluids solutions. Acta Biomater 2009;5:3548–62.
[18] Ebisawa Y, Kokubo T, Ohura K, Yamamuro T. Bioactivity of CaOò-SiO_2 glasses: in vitro evaluation. J Mater Sci Mater Med 1990;1:239–44.
[19] Tilocca A. Review: structural models of bioactive glasses from molecular dynamics simulations. Proc R Soc A 2009;465:1003–27.
[20] Christie JK, Tilocca A. Aluminosilicate glasses as yttrium vectors for in situ radiotherapy: understanding composition-durability effects through molecular dynamics simulations. Chem Mater 2010;22:3725–34.
[21] Tilocca A. Models of structure, dynamics and reactivity of bioglasses: a review. J Mater Chem 2010;20:6848–58.
[22] Vollmayr K, Kob W, Binder K. Cooling-rate effects in amorphous silica: a computer-simulation study. Phys Rev B 1996;54:15808–27.
[23] Jund P, Jullien R. Computer investigation of the energy landscape of amorphous silica. Phys Rev Lett 1999;83:2210–3.
[24] Taraskin SN, Elliott SR. Nature of vibrational excitations in vitreous silica. Phys Rev B 1997;56:8605–22.
[25] Tilocca A, de Leeuw NH. Structural and electronic properties of modified sodium and soda-lime silicate glasses by Car-Parrinello molecular dynamics. J Mater Chem 2006;16:1950–5.
[26] Liang Y, Miranda CR, Scandolo S. Tuning oxygen packing in silica by non-hydrostatic pressure. Phys Rev Lett 2007;75:215504.
[27] Lee TH, Simdyankin SI, Hegedus J, Heo J, Elliott SR. Spatial distribution of rare-earth ions and GaS_4 tetrahedra in chalcogenide glasses studied via laser spectroscopy and ab initio molecular dynamics simulation. Phys Rev B 2000;81:104204.

[28] Du J, Kokou L, Rygel JL, Chen Y, Pantano CG, Woodman R, et al. Structure of cerium phosphate glasses: molecular dynamics simulations. J Am Ceram Soc 2011;94:2393–401.
[29] Ainsworth RI, Di Tommaso D, Christie JK, de Leeuw NH. Polarizable force field development and molecular dynamics study of phosphate-based glasses. J Chem Phys 2012;137:234502.
[30] Tilocca A, de Leeuw NH. Ab initio molecular dynamics study of 45S5 bioactive silicate glass. J Phys Chem B 2006;110:25810–6.
[31] Tilocca A, Cormack AN, de Leeuw NH. The structure of bioactive silicate glasses: new insight from molecular dynamics simulations. Chem Mater 2007;19:95–103.
[32] Christie JK, Tilocca A. Integrating biological activity into radioisotope vectors: molecular dynamics models of yttrium-doped bioactive glasses. J Mater Chem 2012;22:12023–31.
[33] Tilocca A, Cormack AN, de Leeuw NH. The formation of nanoscale structures in soluble phosphosilicate glasses for biomedical applications: MD simulations. Faraday Discuss 2007;136:45–55.
[34] Christie JK, Tilocca A. Molecular dynamics simulations and structural descriptors of radioisotope glass vectors for in situ radiotherapy. J Phys Chem B 2012;116:12614–20.
[35] Christie JK, Ainsworth RI, Di Tommaso D, de Leeuw NH. Nanoscale chains control the solubility of phosphate glasses for biomedical applications. J Phys Chem B 2013;117:10652–7.
[36] Sarnthein J, Pasquarello A, Car R. Structural and electronic properties of liquid and amorphous SiO_2: an ab initio molecular dynamics study. Phys Rev Lett 1995;74:4682–5.
[37] Christie JK, Tilocca A. Short-range structure of yttrium aluminosilicate glass for cancer radiotherapy: Car-Parrinello molecular dynamics simulations. Adv Eng Mater 2010;12:B326–30.
[38] Tang E, Di Tommaso D, de Leeuw NH. An ab initio molecular dynamics study of bioactive phosphate glasses. Adv Eng Mater 2010;12:B331–8.
[39] http://www.cp2k.org.
[40] Perdew JP, Burke K, Ernzerhof M. Generalized gradient approximation made simple. Phys Rev Lett 1996;77:3865–8.
[41] VandeVondele J, Hutter J. Gaussian basis sets for accurate calculations on molecular systems in gas and condensed phases. J Chem Phys 2007;127:114105.
[42] Brauer DS, Al-Noaman A, Hill RG, Doweidar H. Density-structure correlations in fluoride-containing bioactive glasses. Mater Chem Phys 2011;130:121–5.
[43] Pickup DM, Guerry P, Moss RM, Knowles JC, Smith ME, Newport RJ. New sol-gel synthesis of $(CaO)_{0.3}(Na_2O)_{0.2}(P_2O_5)_{0.5}$ bioresorbable glass and its structural characterisation. J Mater Chem 2007;17:4777–84.
[44] Abou Neel EA, Pickup DM, Valappil SP, Newport RJ, Knowles JC. Bioactive functional materials: a perspective on phosphate-based glasses. J Mater Chem 2009;19:690–701.
[45] Brow RK. Review: the structure of simple phosphate glasses. J Non-Cryst Solids 2000;263&264:1–28.
[46] Brow RK, Kirkpatrick RJ, Turner GL. The short range structure of sodium phosphate glasses. I. MAS-NMR studies. J Non-Cryst Solids 1990;116:39–45.
[47] Walter G, Vogel J, Hoppe U, Hartman P. The structure of $CaO\text{-}Na_2O\text{-}MgO\text{-}P_2O_5$ invert glass. J Non-Cryst Solids 2001;296:212–23.
[48] Hoppe U. A structural model for phosphate glasses. J Non-Cryst Solids 1996;195:138–47.
[49] Hoppe U, Walter G, Kranold R, Stachel D. Structural specifics of phosphate glasses probed by diffraction methods: a review. J Non-Cryst Solids 2000;263&264:29–47.
[50] Christie JK, Malik J, Tilocca A. Bioactive glasses as potential radioisotope vectors for in situ cancer therapy: investigating the structural effects of yttrium. Phys Chem Chem Phys 2011;13:17749–55.